

# GABOR-GUIDED TRANSFORMER FOR SINGLE IMAGE DERAINING

*Sijin He, Guangfeng Lin\**

Xi'an University of Technology, China

## ABSTRACT

Image deraining have have gained a great deal of attention in order to address the challenges posed by the effects of harsh weather conditions on visual tasks. While convolutional neural networks (CNNs) are popular, their limitations in capturing global information may result in ineffective rain removal. Transformer-based methods with self-attention mechanisms have improved, but they tend to distort high-frequency details that are crucial for image fidelity. To solve this problem, we propose the Gabor-guided transformer (Gaborformer) for single image deraining. The focus on local texture features is enhanced by incorporating the information processed by the Gabor filter into the query vector, which also improves the robustness of the model to noise due to the properties of the filter. Extensive experiments on the benchmarks demonstrate that our method outperforms state-of-the-art approaches.

**Index Terms**— Image deraining, Gabor filter, transformer, self-attention

## 1. INTRODUCTION

Images captured in adverse rainy conditions can significantly affect the performance of high-level vision tasks. To overcome this challenge, various techniques have been developed to reduce the negative impact of rain on images[1, 2, 3]. Among these methods, convolutional neural networks (CNNs) have received a lot of attention for their excellent ability to learn complex hierarchical features from data.

Many deep learning approaches concentrate on enhancing CNN frameworks, considering them a more desirable option[4, 5, 6, 7, 8]. However, the convolutional operation of CNNs has limitations in processing global information, which makes it difficult to capture long-range correlation between pixels. In recent years, transformer-based methods have made significant progress in the field of image deraining [9, 10, 11]. The self-attention mechanism[12] captures global information more efficiently and improves image distortion caused by rain. Rain-induced image distortion typically involves minute details and textures that are crucial for restoring image clarity and realism. However, we observe that the self-attention mechanism favors focusing on the global information in the image and is relatively poor at processing some high-frequency information (e.g., subtle image textures), as shown in Fig. 1. Therefore, providing the network with relevant high-frequency information can enhance its recovery ability. The standard transformer[12] typically uses a global relationship of query-key pairs to aggregate image features. Both queries and keys are derived by mapping the same input with-

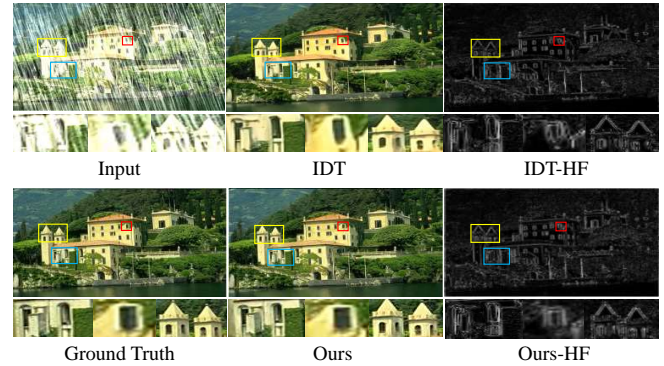


**Fig. 1.** Visual comparison effect of our method with IDT[29]. HF is the visualization result after high-pass filtering. Unlike the IDT, which adds priors to the network structure, our method extract the texture through Gabor, which can recover a finer effect.

out any processing to generate them. The query measures the importance of different locations in the image and it plays a guiding role in computing attention, determining which parts of the input image the model focuses on. The transformer’s performance can be improved through the provision of queries with effective features.

In this study, we propose a new Gabor-guided transformer for image deraining to solve the above problem. Gabor filter are known for its selectivity in multiple scales, directions and frequencies, as well as for its remarkable effect on texture extraction. This flexibility is able to sensitively capture the texture information in the image at different scales and directions, and show robustness to illumination changes[13]. We provide more local texture information to the queries of the self-attention mechanism by using a modified Gabor filter, which tends to focus on regions associated with high-frequency details of the image in the attention computation to enhance attention to local features. In addition, the local texture information extracted by the Gabor filter is usually robust to noise and image changes. By introducing this robustness into the query vector, the self-attention mechanism is better able to resist the effects of noise or subtle changes when computing the attention weights, thus improving the robustness of the model, enabling it to better handle image data from complex environments, and improving the model’s adaptability to imperfect conditions that may occur in real scenes. We apply the cross-channel self-attention mechanism to reduce the computational complexity of the model[14]. Our method outperforms state-of-the-art methods in extensive benchmark experiments.

\*corresponding author

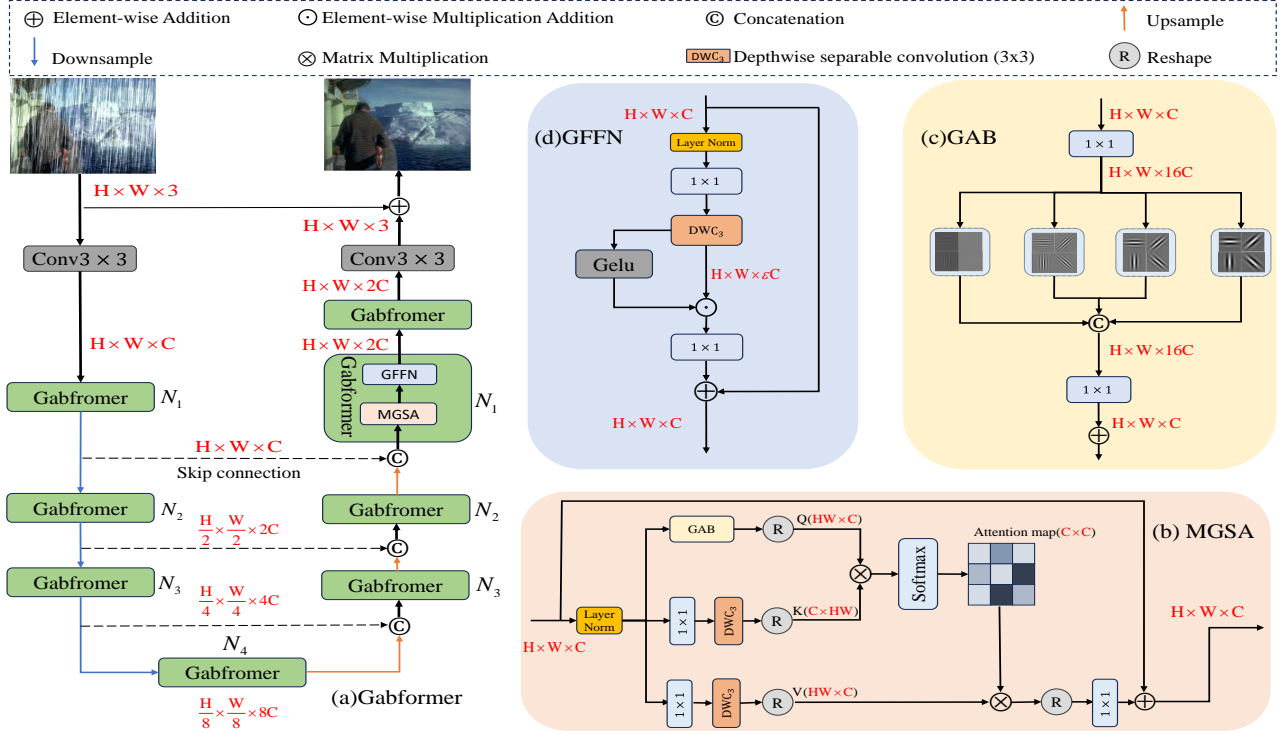


**Fig. 2.** Detailed framework of Gabformer with the main constituent modules of (a) overall framework(Gabformer), (b) Multi-Gabor Self Attention (MGSA), (c) Gabor Filter (GAB), (d) Gated Feed-Forward Network (GFFN)

The main contributions of our paper are summarized as follows:

- We design a multi-scale Gabor texture extraction filter that instructs the network to focus on high-frequency information, allowing the network to acquire richer contextual semantic information that helps recover image structure and texture details.
- We introduce a unique gating module (GFFN) to filter the information, i.e., the unimportant high-frequency information extracted by the Gabor filter is suppressed and only valid information is allowed to pass through the network.
- We have conducted extensive experiments on commonly used benchmark datasets to demonstrate the effectiveness and generalizability of the method. The experiments show that Gabformer can achieve excellent results in a wide range of rain scenes.

## 2. PROPOSED METHOD

### 2.1. Overall pipeline

Specifically, given a rainy image  $I_{in} \in \mathbb{R}^{M \times 3}$ , it is first processed through a generalized convolutional layer along the RGB channel to form low-level feature embeddings  $X_t \in \mathbb{R}^{M \times C}$ , where  $M = H \times W$ ,  $H$  and  $W$  are the height and width of the feature map  $M$ ,  $C$  denotes the number of channels. Feature processing is performed step-by-step by an encoder-decoder model with a 4-level symmetric structure, which each level consists of multiple transformer blocks. In order to extract feature representations layer by layer, spatial size

reduction of the feature map and channel expansion are achieved by stepwise encoding and decoding operations in the adjacent layers of the encoder. Pixel-unshuffle and pixel-shuffle operations[15] are used in the downsampling and upsampling process of the features. In addition, use skip connections[16] to introduce more contextual information and facilitate the flow of information. Finally, the refined features are processed through a convolutional layer and the resulting residual image is summed with the original input image to get the derained image, and the overall pipeline of our Gabformer architecture is shown in Fig 2. Formally, given the input feature  $X_{N-1}$  at the  $(N-1)$ -th block, the definition of the encoding process for Gabformer can be formulated as follows:

$$\begin{aligned} X_N &= \tilde{X}_N + GFFN(l(\tilde{X}_N)), \\ \tilde{X}_N &= X_{N-1} + MGSA(l(X_{N-1})), \end{aligned} \quad (1)$$

where  $l(\cdot)$  is the layer normalization,  $\tilde{X}_N$  and  $X_N$  are output features of the MGSA and GFFN modules.

### 2.2. Multi-Gabor Self Attention

The Gabor filter is a spatial-frequency filter widely employed in the fields of image processing and computer vision, which uniquely combines Gaussian distribution and sinusoidal components to give it both spatial and frequency domain localization properties[35]. This filter responds to a variety of structures in an image at multiple scales and orientations, and exhibits excellent performance in texture and

**Table 1.** Comparison of quantitative results from rain streak datasets, **bold** indicates best results.

Datasets Methods	Rain200L[17]		Rain200H[17]		DDN-Data[18]		DID-Data[19]	
	PSNR	SSIM	PSNR	SSIM	PSNR	SSIM	PSNR	SSIM
DSC[20]	27.16	0.8663	14.73	0.3815	27.31	0.8373	24.24	0.8279
GMM[21]	28.66	0.8652	14.50	0.4164	27.55	0.8479	25.81	0.8344
MSPFN[22]	38.58	0.9827	29.36	0.9034	32.99	0.9333	33.72	0.9550
PRNet[23]	37.80	0.9814	29.04	0.8991	32.60	0.9459	33.17	0.9481
RCDNet[24]	39.17	0.9885	30.24	0.9048	33.04	0.9472	34.08	0.9532
MPRNet[25]	39.47	0.9825	30.67	0.9110	33.10	0.9347	33.99	0.9590
CCN[26]	38.26	0.9812	29.99	0.9138	32.67	0.9252	32.13	0.9238
SPDNet[27]	40.50	0.9875	31.28	0.9207	33.15	0.9457	34.57	0.9560
SwinIR[28]	40.61	0.9871	31.76	0.9151	33.16	0.9312	34.07	0.9313
Restormer[14]	40.99	0.9890	32.00	0.9329	34.20	0.9571	35.29	0.9641
IDT[29]	40.74	0.9884	32.10	0.9344	33.84	0.9549	34.89	0.9623
DRSformer[30]	41.23	0.9894	<b>32.18</b>	<b>0.9330</b>	34.36	0.9590	35.38	<b>0.9647</b>
Ours	<b>41.71</b>	<b>0.9900</b>	31.80	0.9280	<b>34.45</b>	<b>0.9607</b>	<b>35.38</b>	0.9629

**Table 2.** Comparison of quantitative results from a raindrop dataset, **bold** indicates best results.

Methods	Pix2Pix[31]	CMFNet[32]	AttentGAN[33]	CCN[26]	Quan’s[34]	IDT[29]	Ours
PSNR	27.20	31.49	31.59	31.34	31.37	31.63	<b>32.01</b>
SSIM	0.8359	0.9330	0.917	0.9293	0.9183	0.9361	<b>0.9493</b>

edge extraction, it is described as the follows:

$$\begin{aligned}
G(x, y; \lambda, \theta, \psi, \sigma, \gamma) &= \exp\left(-\frac{x'^2 + \gamma^2 y'^2}{2\sigma^2}\right) \cos\left(2\pi \frac{x'}{\lambda} + \psi\right), \\
x' &= x \cos \theta + y \sin \theta, \\
y' &= -x \sin \theta + y \cos \theta,
\end{aligned} \tag{2}$$

where  $x$  and  $y$  are the horizontal and vertical pixel coordinates,  $\lambda$  denotes the filter wavelength,  $\theta$  is the main direction of the filter,  $\psi$  denotes the phase shift,  $\sigma$  is the standard deviation of the Gaussian distribution,  $\gamma$  denotes the spatial ellipticity of the filter,  $x'$  and  $y'$  are the coordinates obtained by rotating  $x$  and  $y$  in the original coordinate system. The larger the wavelength, the wider the range of image structures perceived by the filter, so we used four filters with different wavelengths to enhance adaptability to various scale structures within the image and deepen the overall understanding of the image content. By maintaining fixed values for phase offset, standard deviation, and spatial ellipticity, we ensured that the filter has a consistent texture response in a given direction and frequency. However, image edges often have significant gradients or slopes in one direction due to brightness variations. If only the wavelength is varied without changing the direction, the Gabor filter will be able to detect edges and extract texture in a given direction, which may limit the specificity in different directions. Therefore, we used four directions at each wavelength based on the periodicity of the sine and cosine functions. Superimposing of information from multiple directions and wavelengths gives the model the flexibility to capture edge and texture information in all directions, thus improving the comprehensiveness and robustness of the image analysis.

Inspired by [14], We use cross-channel attention instead of traditional self-attention to save computational complexity. Given a layer normalized input tensor  $X \in \mathbb{R}^{M \times C}$ , we use  $1 \times 1$  convolution for

channel-wise context integration, followed by  $3 \times 3$  depth-wise convolution to capture the spatial context within the channel to obtain the key and value. For query extraction, we use  $1 \times 1$  convolution channel context integration, followed by a Gabor filter with four different wavelengths, each with four orientations, to extract information within the channel dimension, which is given as:

$$Q = f_{1 \times 1} \left( \sum_{i=1}^4 \sum_{j=1}^4 Gab(X, G(\lambda_i, \theta_j)) \right), \tag{3}$$

where  $Q, K$  and  $V$  are of dimension  $\mathbb{R}^{HW \times C}$ ,  $f_{1 \times 1}(\cdot)$  is a  $1 \times 1$  point-by-point convolution,  $G(\cdot)$  stands for the gabor filter function,  $\lambda_i$  and  $\theta_j$  denote the  $i$ -th wavelength and the  $j$ -th direction,  $Gab(\cdot)$  is the filtering operation. Calculating Attention can be expressed as follows:

$$\begin{aligned}
Att(Q, K, V) &= \varphi(Q, K)V, \\
\varphi(Q, K) &= \text{softmax}\left(\frac{K^T Q}{\xi}\right),
\end{aligned} \tag{4}$$

where  $\xi$  is a scale parameter that can be learned to control the size of the attention map. By performing the attentional computation in the channel dimension, we change the computational complexity from  $o(M \times M)$  to  $o(C \times C)$ , which is reduced due to  $M \gg C$ . Similarly, we divide the channels into multiple heads and train attention mappings for each head independently in parallel to improve the model’s ability to capture complex relationships. Eventually, the output  $\tilde{X}$  of the attention can be shown as:

$$\tilde{X} = f_{1 \times 1}(Att(Q, K, V)) + X \tag{5}$$

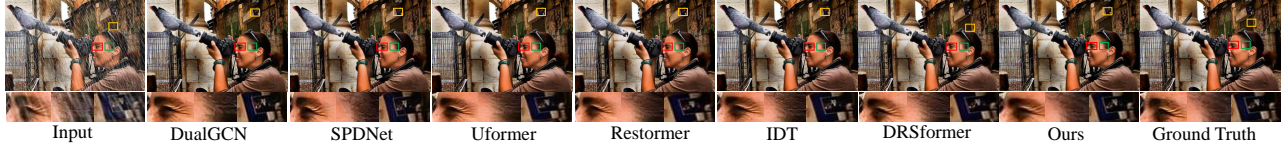


Fig. 3. Comparison of rain removal visualization on the Rain200L dataset, zoom in for clearer view of effectiveness.



Fig. 4. Comparison of rain removal visualization on the AGAN-Data dataset, zoom in for clearer view of effectiveness.

### 2.3. Gating Feed-Forward Network

Although we effectively reduce the computational complexity of the model by introducing cross-channel attention, this is accompanied by the use of a Gabor filter to extract texture features, which introduces additional computational overhead. In order to improve information transfer efficiency while reducing computational costs, we introduce a gating module[14] to replace the FFN. Given an input feature  $\tilde{X} \in \mathbb{R}^{M \times C}$ , subsequent to layer normalization, we use a  $1 \times 1$  convolution to expand the channel by a ratio of  $\varepsilon$ , then it is fed into two parallel paths, both paths are convolved with  $3 \times 3$  deep-wise convolution to extract the local information, and one of them is activated with a *GELU* for gating action. The final output is made by superimposing the features of the two paths, the whole process of fusing features is represented as

$$\begin{aligned} \hat{X} &= d_{3 \times 3}(f_{1 \times 1}(l(\tilde{X}))) \\ X &= \tilde{X} + \hat{X} \odot GELU(\hat{X}) \end{aligned} \quad (6)$$

where  $\tilde{X}$  denotes the output of the Multi-Gabor Self Attention,  $d_{3 \times 3}(\cdot)$  is a  $3 \times 3$  deep-wise convolution,  $\odot$  is the element-wise multiplication, and  $X$  represents the output of the GFFN.

## 3. EXPERIMENTAL RESULTS

### 3.1. Experimental Settings

**datasets.** Our experiments include five public benchmark datasets. The rain streak datasets include Rain200L[17], Rain200H[17], DID-Data[19] and DDN-Data[18]. In addition, we evaluated the performance of the model using a raindrop dataset, *i.e.*, AGAN-Data[36].

**Implementation Details.** We used PSNR and SSIM to quantitatively evaluate the performance of the method. In our model,  $\{N_1, N_2, N_3, N_4\}$  in Fig. 2 are  $\{4, 6, 6, 8\}$ , respectively. The initial learning rate is set to  $3 \times 10^{-4}$  and decreases using a cosine annealing scheme to  $1 \times 10^{-6}$  after 92,000 iterations, followed by another 208,000 iterations of model training. In the Gabor filter,  $\sigma$  is set to  $2\pi$ ,  $\psi$  is 0,  $\gamma$  is 0.5,  $\{\lambda_1, \lambda_2, \lambda_3, \lambda_4\}$  and  $\{\theta_1, \theta_2, \theta_3, \theta_4\}$  are  $\{1.0, 1.5, 2.0, 2.5\}$  and  $\{45^\circ, 90^\circ, 135^\circ, 180^\circ\}$ , respectively. Table 3 shows the effect of using filters with different wavelengths and orientations on the rain removal effect of the image. From Table 3, the effect is significantly improved by superimposing multiple wavelengths and directions.

Table 3. Parametric sensitivity analysis, we employed diverse Gabor filter with different wavelengths and orientations, comparing PSNR on the Rain200L dataset to evaluate feature extraction performance.

Metric	$\theta_1$	$\theta_2$	$\theta_3$	$\theta_4$	$\theta_1, \theta_2, \theta_3, \theta_4$
$\lambda_1$	41.42	41.30	41.13	41.37	41.06
$\lambda_2$	41.30	41.22	41.41	41.15	41.29
$\lambda_3$	41.20	41.15	41.41	41.35	41.48
$\lambda_4$	41.16	41.21	41.17	41.35	41.36
$\lambda_1, \lambda_2, \lambda_3, \lambda_4$	41.51	41.63	41.48	41.35	<b>41.71</b>

**Quantitative Evaluation.** We compare our Gabformer with the state-of-the-art methods, including two prior-based models (DSC[20] and GMM[21]), as well as CNN-based approaches (including MSPFN[22], PReNet[23], RCDNet[24], MPRNet[25], CCN[26], and SPDNet[27]). In addition, we examine recent Transformer-based approaches, including Uformer[37], SwinIR[28], Restormer[14], IDT[29], DRSformer[30]. For raindrop removal, we compare CMFNet[32], Pix2Pix[31], Atten-tGAN[33], Quan's network[34], CCN[26] and IDT[29]. Table 1 shows the results of comparing our method with the SoTA method for rain streak datasets, and Table 2 shows the comparison results for raindrop datasets. We can see that our method achieves much better performance on most datasets from Table 1 and Table 2. In addition, Fig. 3 and Fig. 4 show the rain removal effect of the images in the two datasets, which also demonstrate that our method has better recovery results.

### 3.2. Ablation Study

In this section, we evaluate the performance of the proposed Gabformer. Specifically, we evaluate the impact on queries of both adding the Gabor filter to extract texture features and feature extraction by depthwise separable convolution. Furthermore, validation is performed to compare the difference between the case where texture features are extracted by adding the Gabor filter only to  $Q_G$  and the case where the gabor filter is applied to  $Q_G, K_G, V_G$ . In addition, it has been mentioned that using the relu function instead of the softmax can generate sparse attention maps to effectively exclude irrelevant features[38], and we also conducted experiments. The experimental results are shown in Table 4. From table 4, our proposed

Gabformer has the best performance.

**Table 4.** Ablation study on the Rain200L dataset for image deraining with different network configurations

Network Configuration	PSNR	SSIM
$Q, K, V + GFFN$	40.99	0.9890
$Q_G, K_G, V_G + softmax + GFFN$	41.28	0.9897
$Q_G, K_G, V_G + RELU + GFFN$	39.17	0.9849
$Q_G, K, V + RELU + GFFN$	41.00	0.9890
$Q_G, K, V + softmax + FFN$	39.28	0.9848
$Q_G, K, V + softmax + GFFN$	<b>41.73</b>	<b>0.9900</b>

### 3.3. Experimental Analysis

In this study, we investigate the effectiveness of the multi-scale Gabor filter by varying the combination of wavelengths and directions, and the experimental results are shown in Table 3. The experimental results show that the filter with a mixture of multiple wavelengths and directions has better performance in image processing. This demonstrates the importance of multiscale information, as this mixture captures the features in the image more comprehensively. However, we also observe that certain specific combinations (e.g.,  $[\lambda_1, \theta_1]$ ) are able to produce more pronounced results at certain angles or scales. This may be due to the fact that the image has more significant gradients at these angles or scales, making the particular combination of filter more effective. Overall, the filter with a mixture of several wavelengths and directions is still the best choice.

We use the texture information extracted by Gabor as queries, and use depthwise separable convolution to encode spatially localized contextual information as keys and values, which allows the network to focus on more contextual semantic information in the image, improving the network’s localization and globalization.

By using the Gabor filter, more high frequency information is given to the network, but not all of the high frequency information contributes to the image deraining, so we use a gated module (GFFN). The last two rows of the ablation experiments in Table 4 show the difference between the modules used. As can be seen in Table 4, the gated module effectively suppresses the less important information in the channel and allows the effective high frequency information to be delivered, resulting in excellent performance with a reduced number of network parameters.

## 4. CONCLUSIONS

In this study, we propose a new Gabor-based transformer for single image deraining. Specifically, we design multi-scale and multi-directional combined the Gabor filter to extract image texture features and use them as queries for the attention mechanism to increase the network’s attention to the detailed information of the image, which improves the deraining effect. In addition, by extracting texture features in the image channel dimension to reduce the computational complexity, our Gabformer can also be applied to high-resolution images. A large number of experiments surface that our proposed method works better than the SoTA method. However, the addition of Gabor filter introduces an additional number of parameters into the model. Our model has 34.4M parameters, which may

be difficult to deploy on resource-limited devices, and we will effectively filter the useful high and low frequency information of the image in our model, using pruning or distillation to reduce the number of parameters of the model along with good performance.

## 5. REFERENCES

- [1] Xin Jin, Zhibo Chen, Jianxin Lin, Zhikai Chen, and Wei Zhou, “Unsupervised single image deraining with self-supervised constraints,” in *ICIP*, 2019, pp. 2761–2765.
- [2] Yuto Namba, Jiande Sun, and Xian-Hua Han, “Coupling spatial and channel transformer for single image deraining,” in *ICIP*, 2023, pp. 2080–2084.
- [3] Yu Luo, Yong Xu, and Hui Ji, “Removing rain from a single image via discriminative sparse coding,” in *ICCV*, 2015, pp. 3397–3405.
- [4] Xiang Chen, Jinshan Pan, Kui Jiang, Yufeng Li, Yufeng Huang, Caihua Kong, Longgang Dai, and Zhentao Fan, “Unpaired deep image deraining using dual contrastive learning,” in *CVPR*, 2022, pp. 2007–2016.
- [5] Dongwei Ren, Wangmeng Zuo, Qinghua Hu, Pengfei Zhu, and Deyu Meng, “Progressive image deraining networks: A better and simpler baseline,” in *CVPR*, 2019, pp. 3932–3941.
- [6] Kui Jiang, Zhongyuan Wang, Peng Yi, Chen Chen, Baojin Huang, Yimin Luo, Jiayi Ma, and Junjun Jiang, “Multi-scale progressive fusion network for single image deraining,” in *CVPR*, 2020, pp. 8343–8352.
- [7] Qiaosi Yi, Juncheng Li, Qinyan Dai, Faming Fang, Guixu Zhang, and Tiejong Zeng, “Structure-preserving deraining with residue channel prior guidance,” in *ICCV*, 2021, pp. 4218–4227.
- [8] Pengpeng Li, Jiyu Jin, Guiyue Jin, Lei Fan, Xiao Gao, Tianyu Song, and Xiang Chen, “Deep scale-space mining network for single image deraining,” in *CVPRW*, 2022, pp. 4275–4284.
- [9] Hanting Chen, Yunhe Wang, Tianyu Guo, Chang Xu, Yiping Deng, Zhenhua Liu, Siwei Ma, Chunjing Xu, Chao Xu, and Wen Gao, “Pre-trained image processing transformer,” in *CVPR*, 2021, pp. 12294–12305.
- [10] Jeya Maria Jose Valanarasu, Rajeev Yasarla, and Vishal M. Patel, “Transweather: Transformer-based restoration of images degraded by adverse weather conditions,” in *CVPR*, 2022, pp. 2343–2353.
- [11] Zhendong Wang, Xiaodong Cun, Jianmin Bao, Wengang Zhou, Jianzhuang Liu, and Houqiang Li, “Uformer: A general u-shaped transformer for image restoration,” in *CVPR*, 2022, pp. 17662–17672.
- [12] Ashish Vaswani, Noam Shazeer, Niki Parmar, Jakob Uszkoreit, Llion Jones, Aidan N Gomez, Łukasz Kaiser, and Illia Polosukhin, “Attention is all you need,” in *NeurIPS*, 2017, vol. 30.
- [13] Meharg Rai and Pablo Rivas, “A review of convolutional neural networks and gabor filters in object recognition,” in *CSCI*, 2020, pp. 1560–1567.

- [14] Syed Waqas Zamir, Aditya Arora, Salman Khan, Munawar Hayat, Fahad Shahbaz Khan, and Ming-Hsuan Yang, "Restormer: Efficient transformer for high-resolution image restoration," in *CVPR*, 2022, pp. 5728–5739.
- [15] Wenzhe Shi, Jose Caballero, Ferenc Huszár, Johannes Totz, Andrew P. Aitken, Rob Bishop, Daniel Rueckert, and Zehan Wang, "Real-time single image and video super-resolution using an efficient sub-pixel convolutional neural network," in *CVPR*, 2016, pp. 1874–1883.
- [16] Olaf Ronneberger, Philipp Fischer, and Thomas Brox, "U-net: Convolutional networks for biomedical image segmentation," in *MICCAI*, 2015, pp. 234–241.
- [17] Wenhan Yang, Robby T Tan, Jiashi Feng, Jiaying Liu, Zongming Guo, and Shuicheng Yan, "Deep joint rain detection and removal from a single image," in *CVPR*, 2017, pp. 1357–1366.
- [18] Xueyang Fu, Jiabin Huang, Delu Zeng, Yue Huang, Xinghao Ding, and John Paisley, "Removing rain from single images via a deep detail network," in *CVPR*, 2017, pp. 3855–3863.
- [19] He Zhang and Vishal M Patel, "Density-aware single image de-raining using a multi-stream dense network," in *CVPR*, 2018, pp. 695–704.
- [20] Yu Luo, Yong Xu, and Hui Ji, "Removing rain from a single image via discriminative sparse coding," in *ICCV*, 2015, pp. 3397–3405.
- [21] Yu Li, Robby T Tan, Xiaojie Guo, Jiangbo Lu, and Michael S Brown, "Rain streak removal using layer priors," in *CVPR*, 2016, pp. 2736–2744.
- [22] Kui Jiang, Zhongyuan Wang, Peng Yi, Chen Chen, Baojin Huang, Yimin Luo, Jiayi Ma, and Junjun Jiang, "Multi-scale progressive fusion network for single image deraining," in *CVPR*, 2020, pp. 8346–8355.
- [23] Dongwei Ren, Wangmeng Zuo, Qinghua Hu, Pengfei Zhu, and Deyu Meng, "Progressive image deraining networks: A better and simpler baseline," in *CVPR*, 2019, pp. 3937–3946.
- [24] Hong Wang, Qi Xie, Qian Zhao, and Deyu Meng, "A model-driven deep neural network for single image rain removal," in *CVPR*, 2020, pp. 3103–3112.
- [25] Syed Waqas Zamir, Aditya Arora, Salman Khan, Munawar Hayat, Fahad Shahbaz Khan, Ming-Hsuan Yang, and Ling Shao, "Multi-stage progressive image restoration," in *CVPR*, 2021, pp. 14821–14831.
- [26] Ruijie Quan, Xin Yu, Yuanzhi Liang, and Yi Yang, "Removing raindrops and rain streaks in one go," in *CVPR*, 2021, pp. 9147–9156.
- [27] Qiaosi Yi, Juncheng Li, Qinyan Dai, Faming Fang, Guixu Zhang, and Tiejong Zeng, "Structure-preserving deraining with residue channel prior guidance," in *CVPR*, 2021, pp. 4238–4247.
- [28] Jingyun Liang, Jie Zhang Cao, Guolei Sun, Kai Zhang, Luc Van Gool, and Radu Timofte, "Swinir: Image restoration using swin transformer," in *ICCV*, 2021, pp. 1833–1844.
- [29] Jie Xiao, Xueyang Fu, Aiping Liu, Feng Wu, and Zheng-Jun Zha, "Image de-raining transformer," *IEEE TPAMI*, 2022.
- [30] Xiang Chen, Hao Li, Mingqiang Li, and Jinshan Pan, "Learning a sparse transformer network for effective image deraining," in *CVPR*, 2023, pp. 5896–5905.
- [31] Phillip Isola, Jun-Yan Zhu, Tinghui Zhou, and Alexei A Efros, "Image-to-image translation with conditional adversarial networks," in *CVPR*, 2017, pp. 1125–1134.
- [32] Chi-Mao Fan, Tsung-Jung Liu, and Kuan-Hsien Liu, "Compound multi-branch feature fusion for image deraindrop," in *ICIP*, 2023, pp. 3399–3403.
- [33] Rui Qian, Robby T Tan, Wenhan Yang, Jiajun Su, and Jiaying Liu, "Attentive generative adversarial network for raindrop removal from a single image," in *CVPR*, 2018, pp. 2482–2491.
- [34] Yuhui Quan, Shijie Deng, Yixin Chen, and Hui Ji, "Deep learning for seeing through window with raindrops," in *ICCV*, 2019, pp. 2463–2471.
- [35] Rajiv Mehrotra, Kameswara Rao Namuduri, and Nagarajan Ranganathan, "Gabor filter-based edge detection," *Pattern recognition*, vol. 25, no. 12, pp. 1479–1494, 1992.
- [36] Rui Qian, Robby T Tan, Wenhan Yang, Jiajun Su, and Jiaying Liu, "Attentive generative adversarial network for raindrop removal from a single image," in *CVPR*, 2018, pp. 2482–2491.
- [37] Zhendong Wang, Xiaodong Cun, Jianmin Bao, Wengang Zhou, Jianzhuang Liu, and Houqiang Li, "Uformer: A general u-shaped transformer for image restoration," in *CVPR*, 2022, pp. 17683–17693.
- [38] Wenli Huang, Ye Deng, Siqi Hui, Yang Wu, Sanping Zhou, and Jinjun Wang, "Sparse self-attention transformer for image inpainting," *Pattern Recognition*, vol. 145, pp. 109897, 2024.